Supplementary Information for

Constructing Orderly Crystal Orientation with Bidirectional Coordinator for High Efficiency and Stable Perovskite Solar Cells

Jaehwi Lee,‡[a] *Yun Seop Shin,*‡[ab] *Elham Oleiki,*‡[c] *Jongdeuk Seo,*[a] *Jina Roe,*[a] *Dongmin Lee,*[b] *YeonJeong Lee,*[a] *Taehee Song,*[a] *Hyungsu Jang,*[a] *Ji Won Song,*[b] *Woosuk Lee,*[b] *Geunsik Lee,**[c] *Jin Young Kim,**[ab] *Dong Suk Kim**[ab]

[a] School of Energy and Chemical Engineering, Ulsan National Institute of Science and Technology (UNIST), Ulsan 44919, Republic of Korea. E-mail: jykim@unist.ac.kr

[b] Graduate School of Carbon Neutrality, Ulsan National Institute of Science and Technology (UNIST), Ulsan 44919, Republic of Korea. E-mail: kimds@unist.ac.kr

[c] Center for Superfunctional Materials, Department of Chemistry, Ulsan National Institute of Science and Technology (UNIST), Ulsan 44919, Republic of Korea. E-mail: gslee@unist.ac.kr

‡ These authors equally contributed to this work

* Corresponding author. E-mail: gslee@unist.ac.kr, jykim@unist.ac.kr, kimds@unist.ac.kr

Experimental Section

Materials

Fluorine-doped tin oxide on glass (FTO glass, 7 Ω sq^{-1}) was purchased from Asahi. Hydrogen peroxide (H_2O_2, electronic grade), ethanol (EtOH, 95%, special grade) and ethyl ether (99.5%, special grade) were purchased from SAMCHUN. Hydrochloride (HCl, 37 wt% in water) was purchased from Junsei Chemical Co. Methylammonium chloride (MACl, for synthesis), *N,N*-dimethylformamide (DMF, anhydrous 99.8%), dimethyl sulfoxide (DMSO, >99.5%), 2-propanol (IPA, anhydrous, 99.5%), 2-methoxyethanol (2-ME, anhydrous, 99.8%), acetonitrile (anhydrous, 99.8%), chlorobenzene (CB, anhydrous, 99.8%), titanium diisopropoxide bis(acetylacetonate) (Ti(acac)$_2$, 75 wt% in isopropanol), potassium chloride (KCl, ACS reagent, 99.999% trace metals basis), cesium formate (CsFo, 98%), cesium acetate (CsAc, ≥99.99% trace metal basis), cesium trifluoroacetate (CsTFA, BioUltra, ≥99.0%), 4-*tert*-butylpyridine (*t*BP, 98%), and bis(trifluoromethane)sulfonimide lithium salt (LiTFSI) were purchased from Sigma-Aldrich. Tin(IV) oxide (SnO$_2$, 15% in H_2O colloidal dispersion) was purchased from Thermo Fisher Scientific. Lead(II) iodide (PbI$_2$, 99.99% trace metal basis) was purchased from TCI. Formamidinium iodide (FAI) and *n*-octylammonium iodide (OAI) were purchased from Greatcell Solar Materials. Spiro-OMeTAD (99.5%) and FK209 Co(III) TFSI salt (>99%) were purchased from Lumtec.

Materials Synthesis

Formamidinium lead triiodide (FAPbI$_3$) black powder was synthesized by mixing FAI (0.8M) with PbI$_2$ (1:1 molar ratio) in 2-ME with stirring. The mixture was heated to 120 ℃ with a stirring bar, and then recrystallized by adding CB dropwise into the mixture. Finally, the precipitated FAPbI$_3$ powder was filtered using a glass filter and baked at 150 ℃ for 30 min.

PSCs Fabrication

FTO glass was cleaned following the RCA-SC2 procedure using blends of H_2O_2, HCl, and H_2O, and subsequently, acetone and IPA were used sequentially in an ultrasonic bath. The compact TiO$_2$ (c-TiO$_2$) solution was prepared by diluting Ti(acac)$_2$ in EtOH (with 1:15 v/v %), followed by deposition onto FTO substrates using the spray coating method under 450 ℃ conditions. These substrates were annealed at 450 ℃ for 1 h to achieve the desired crystallinity of TiO$_2$. To prepare a bilayer with a structure of c-TiO$_2$/SnO$_2$, the diluted SnO$_2$ nanoparticles

were coated onto the c-TiO$_2$ substates, and subsequently annealed at 100 °C for 1 h in a vacuum oven. Following this, a solution of 4 mg/mL KCl in DI water was spin-coated at 3000 rpm for 30 s and annealed at 100 °C for 30 min. Before use, the substrates were stored in a vacuum oven with 100 °C for 1–2 days. For the target substrate, prior to depositing perovskite films, CsX in DI water was spin-coated at 3000 rpm for 30 s and annealed at 150 °C for 15 min. The perovskite precursor solution was prepared by mixing 1,202 mg FAPbI$_3$, 35 mol% MACl, and 0.8 mol% MAPbBr$_3$ in a mixture of DMF and DMSO (4:1). The filtered perovskite solution, using a 0.2 μm PVDF filter, was spread over the as-prepared bilayer substrate at 7,500 rpm for 50 s with a ramping duration of 0.1 s. During the spin-coating process, 1 mL of diethyl ether, serving as an anti-solvent, was dripped after spinning for 10 s, followed by immediate annealing on a hot plate at 150 °C for 15 min and 100 °C for 30 min sequentially. To passivate the surface of the perovskite, 4 mg/mL of OAI dissolved in IPA was spin-coated on top of the perovskite film at 3,000 rpm for 30 s. After then, the hole-transporting layer was deposited by spin-coating a spiro-OMeTAD (113.9 mg/mL, Lumtech) solution, containing varying dopant ratios of tBP, LiTFSI, and FK209 Co(III) TFSI salt, at 4,000 rpm for 30 s. Finally, a gold electrode (70 nm) was deposited by thermal evaporation under high vacuum of 10^{-6} Torr.

DFT Calculation Details

DFT calculations were performed using the Vienna Ab initio Simulation Package (VASP) suite, which is based on the plane wave pseudopotential approach.[1] The generalized gradient approximation (GGA) within the Perdew-Burke-Ernzerhof (PBE) parameterization was utilized as the exchange-correlation functional.[2] Furthermore, van der Waals (vdW) interactions were incorporated by adding dispersion correction to the total energy and forces by employing the DFT-D3 approach.[3] To model the FAPbI$_3$ (001) surface, the cubic phase is considered with an experimentally determined lattice parameter of a = 6.36 Å.[4] The 1×1 and 2×2 slabs, including four-unit cells along the [001] direction, were considered for HCO$_2$, CH$_3$CO$_2$, and CF$_3$CO$_2$ adsorption on the ideal and defective perovskite surface, respectively. A vacuum layer of ~15 Å was provided to avoid spurious interactions between the periodic images. Structural optimization was performed on 3×3×1 and 2×2×1 k-meshes for the ideal and defective perovskite surfaces, respectively, with a kinetic energy cutoff of 400 eV. The convergence criteria of 10^{-4} eV and 0.01 eV Å^{-1} was employed for energies and forces, respectively. The density of state calculation was performed on a 3×3×1 k-mesh with 10^{-6} eV convergence criteria of energy. The concentration of 10^{14} molecules cm^{-2} was considered for

the ideal surface coverage. The surface defect concentration of 10^{13} cm^{-2} was introduced to the perovskite surface. For molecular adsorption sites, four high symmetry positions were considered, which are referenced with respect to the position of the molecular CH, CH$_3$, and CF$_3$ on the FAPbI$_3$ surface, i.e., Pb top (Pb$_{top}$), I top (I$_{top}$), hollow site on top of surface FA ions, and bridge position between the Pb and I atoms.

The molecular adsorption energy (E_{ad}) is defined as E_{ad} = E(molecule/FAPbI$_3$) – E(FAPbI$_3$) – E(molecule), where E(molecule/FAPbI$_3$), E(FAPbI$_3$), and E(molecule) correspond to the total energies of the combined molecule/FAPbI$_3$ system, FAPbI$_3$ slab, and isolated molecule, respectively.

Characterization of Perovskite Films

UV absorption spectra were carried out using a spectrophotometer (Cary 5000, Agilent). PL spectra were obtained using a fluorometer with xenon lamp as an excitation source (nF900, Edinburgh Instruments). The TRPL spectra were measured using a time-correlated single-photon counting (TCPSC) spectrometer (FluoTime 300, PciQuant). The samples were photoexcited at 510 nm using a pulsed diode laser head (LDH-D-C-510, PicoQuant). AFM images were measured with a microscope (Dimension ICON, Bruker Nano Surface). FTIR spectra were measured using a spectrometer with attenuated total reflection mode (670-IR, Varian). XPS and UPS spectra were measured using a spectrometer (ESCALAB 250XI, Thermo Fisher Scientific) at a base pressure of 1.0×10^{-9} Torr with a monochromated Al-Kα X-ray source. UPS samples were prepared on thermally evaporated Au substrates. Surface contact angles were obtained using a high-speed camera (Fastcam Mini UX50, Photron) with a goniometer (DSA100, KRUSS GmbH). Cross-sectional SEM images were obtained with a cold field-emission scanning electron microscope (S-4800, Hitachi High-Tech.). XRD patterns of the perovskite films were measured using a diffractometer (D8 ADVANCE, Bruker AXS) equipped with Cu-Kα radiation, (λ = 0.1542 nm) as the X-ray source. GIXRD patterns and rocking curves of the perovskite films were performed using a diffractometer (D8 DISCOVERY, Bruker) equipped with Cu-Kα radiation, (λ = 0.1542 nm) as the X-ray source.

Characterization of Charge-Carrier Dynamics

Electrical conductivities of CsX-treated SnO$_2$ were evaluated by measuring the *J-V* curves with the structure of ITO/SnO$_2$/CsX/Au, where ITO represents indium tin oxide. Mott-Schottky curves were measured using a potentiostat (VMP3/VSP-300, BioLogic) in the 0-1.3

4

V voltage range and at a frequency of 0.5 MHz under dark conditions. EIS curves of PSCs were measured using a potentiostat (WIZEIS-1200premium, WizMAC) under dark conditions.

Characterization of PSCs

PSCs underwent measurements utilizing a solar simulator (Newport-Oriel 94083A, Class AAA) in conjunction with a Keithley source meter 2400, under ambient conditions (20% RH at 25 °C). The light intensity was calibrated to 100 mW cm^{-2} employing a Si-reference cell certified by the National Renewable Energy Laboratory. To mitigate artifacts induced by scattered light, a non-reflective mask with an aperture area of 0.0802 cm^2 was used to shield the active area of the device. The conventional *J-V* curves were measured under both forward (from a forward bias (-0.05 V) to a short circuit (1.30 V)) and reverse (from a forward bias (1.30 V) to a short circuit (-0.05 V)) scans with the fixed step voltage of 20 mV. EQEs were measured using a quantum efficiency measurement system (QUANTX-300, Newport Co.)
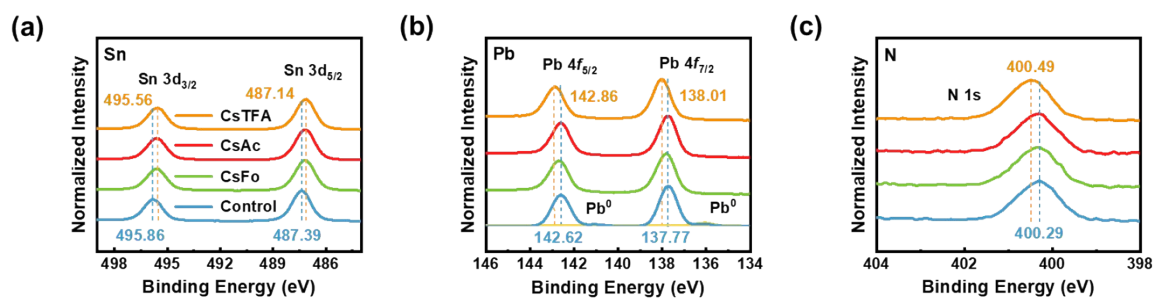
Fig. S1 XPS spectra corresponding to (a) Sn 3d of the control- and CsX-treated SnO_2, (b) Pb 4f and (c) N 1s of the perovskite films that were peeled off from the control- and CsX-treated SnO_2.
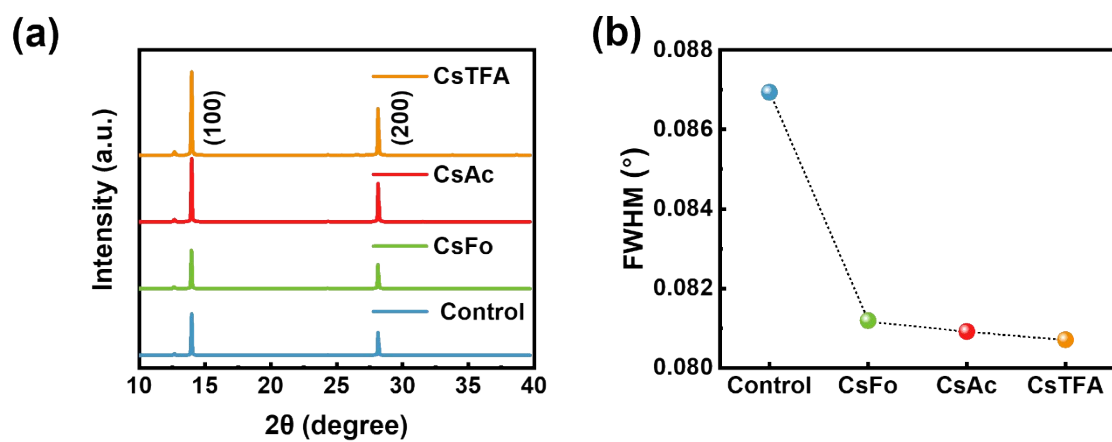
Fig. S2 (a) XRD patterns of the deposited perovskite films on the control- and CsX-treated SnO$_2$. (b) FWHM of (001) crystal diffraction peak obtained from the XRD patterns of the perovskite films.
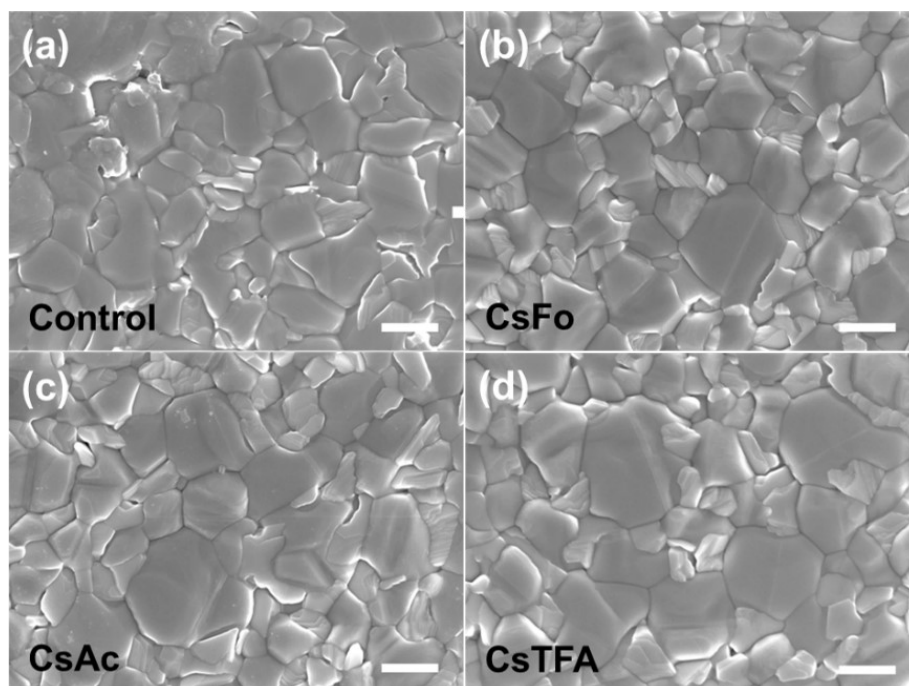
Fig. S3 Top-view SEM images of the perovskite films deposited on the control- and CsX-treated SnO_2. (The scale bar is 1 µm).
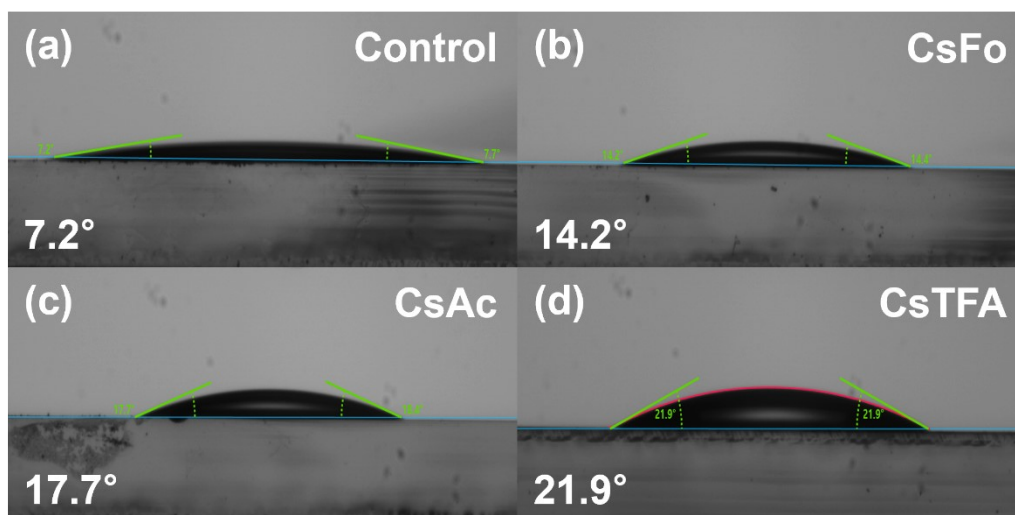
Fig. S4 The contact angles of water droplet on the control- and CsX-treated SnO$_2$.
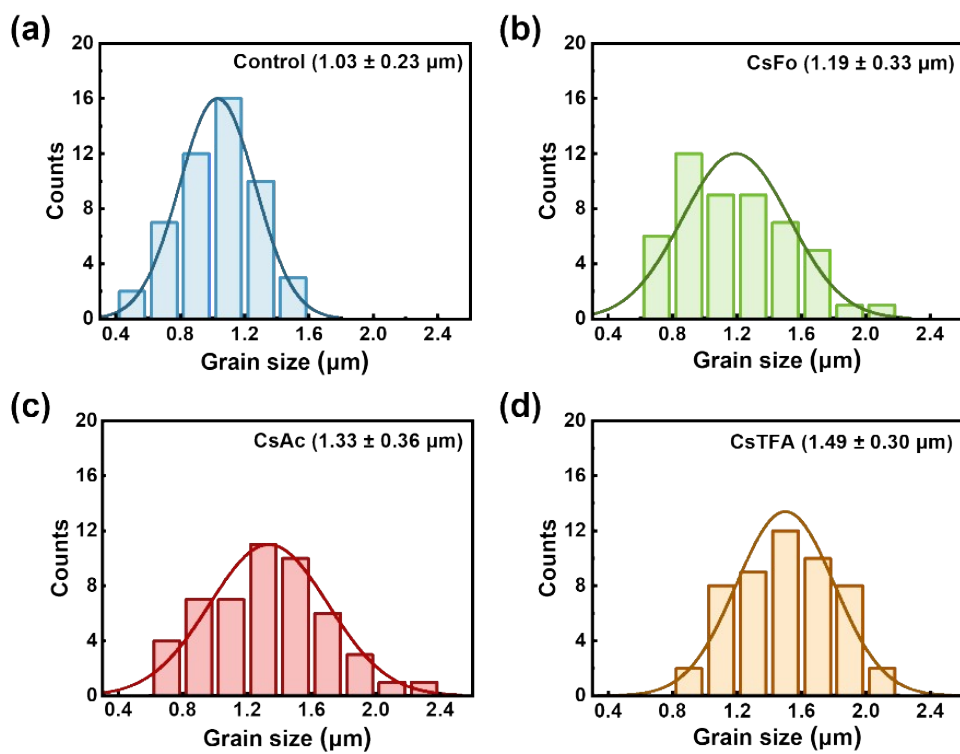
Fig. S5 The distribution of grain sizes of the perovskite films deposited on the control- and CsX-treated SnO_2.
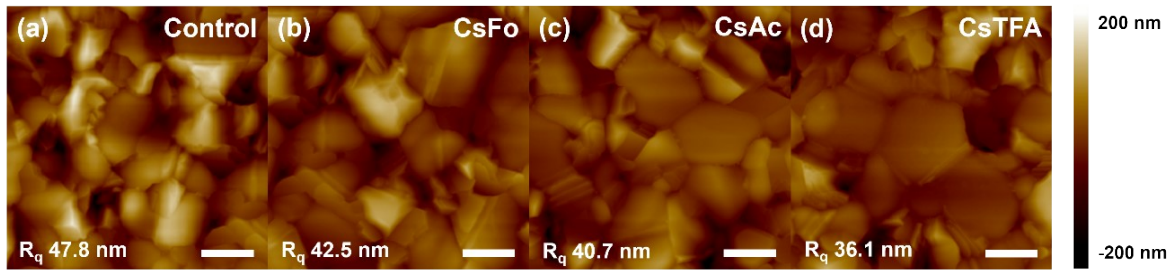
Fig. S6 AFM images of the perovskite films deposited on the control- and CsX-treated SnO_2. (The scale bar is 1 μm).
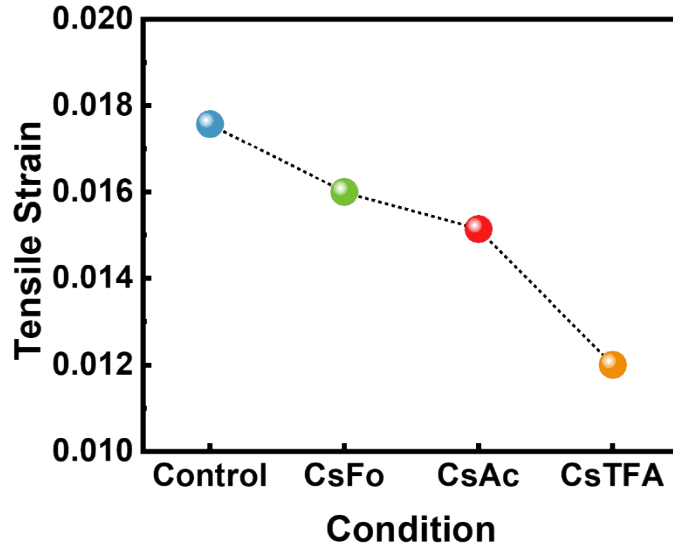
Fig. S7 Tensile strain values obtained from GIXRD measurements of the perovskite films deposited on the control- and CsX-treated SnO$_2$. We calculated the tensile strain values within the perovskite films using the following the equation[5]:

$$\sigma = -\frac{E}{2(1+v)}\frac{\pi}{180}\cot\theta_0\frac{\partial(2\theta)}{\partial\sin^2(\psi)} \qquad \varepsilon = \frac{\sigma}{E}$$

ε: strain, σ: stress (Pa=N/m^2), E: Young's modulus (9.90 for FAPbI$_3$, Pa=N/m^2),[6] v: Poisson's ratio (0.40 for FAPbI$_3$),[6] θ_0: strain-free angle, θ: incident angle, $\psi(=\omega)$: angle the diffraction vector
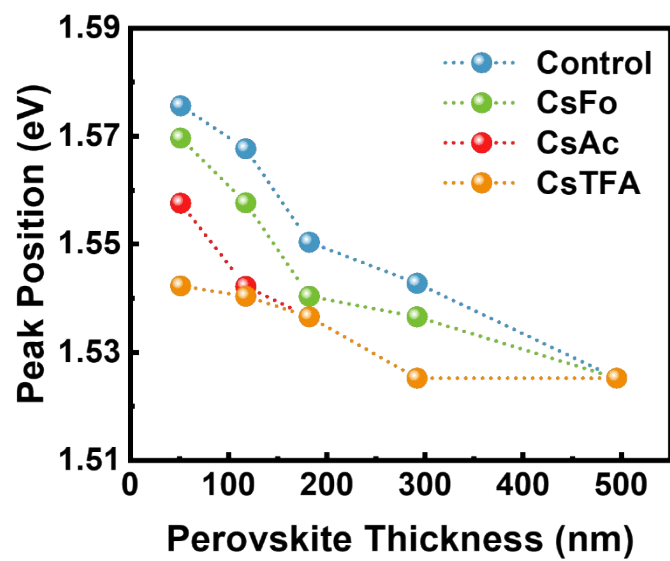
Fig. S8 The variation of PL peak positions with varying the thickness of the perovskite films deposited on the control- and CsX-treated SnO$_2$.
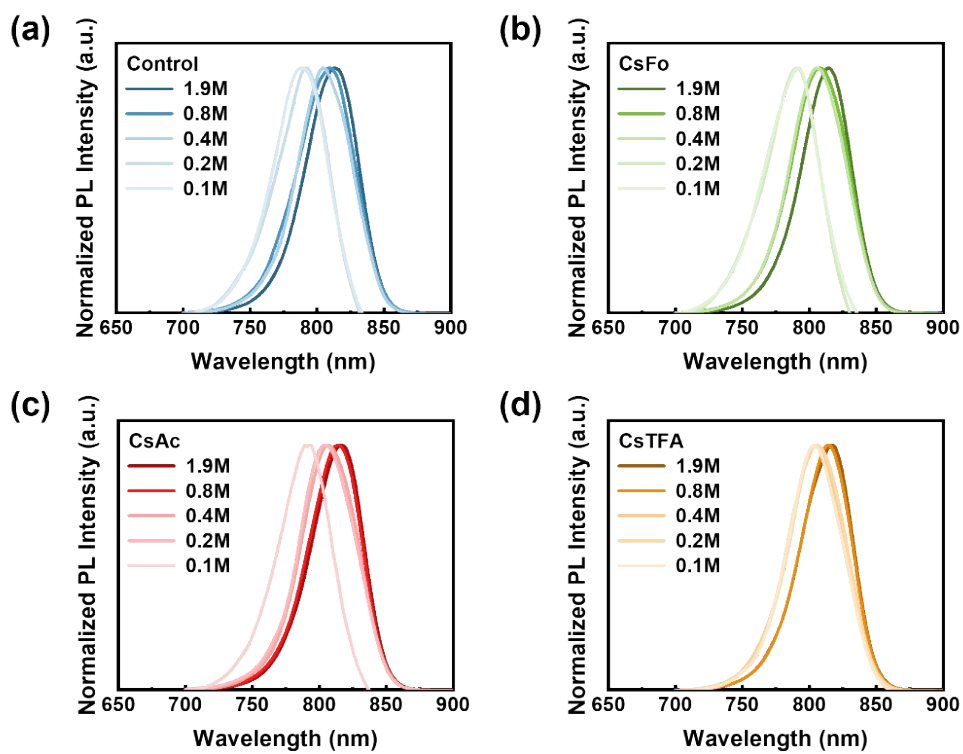
Fig. S9 Normalized PL spectra with varying the thickness of the perovskite films deposited on the control- and CsX-treated SnO_2.
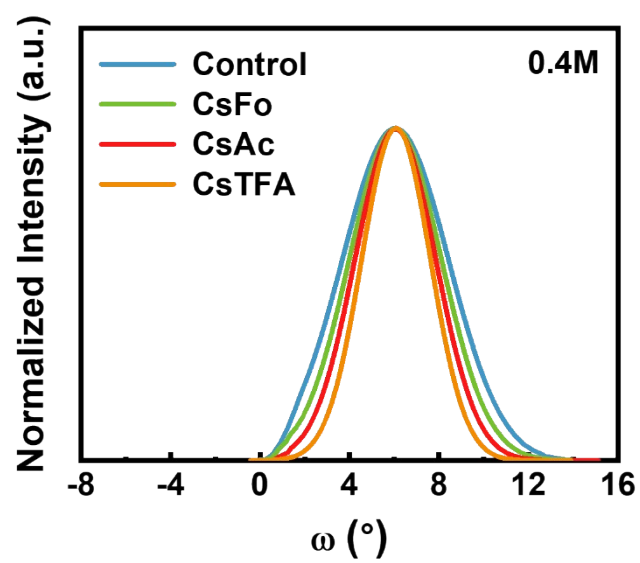
Fig. S10 XRD rocking curves of the perovskite films (with a concentration of 0.4M) deposited on the control- and CsX-treated SnO_2.
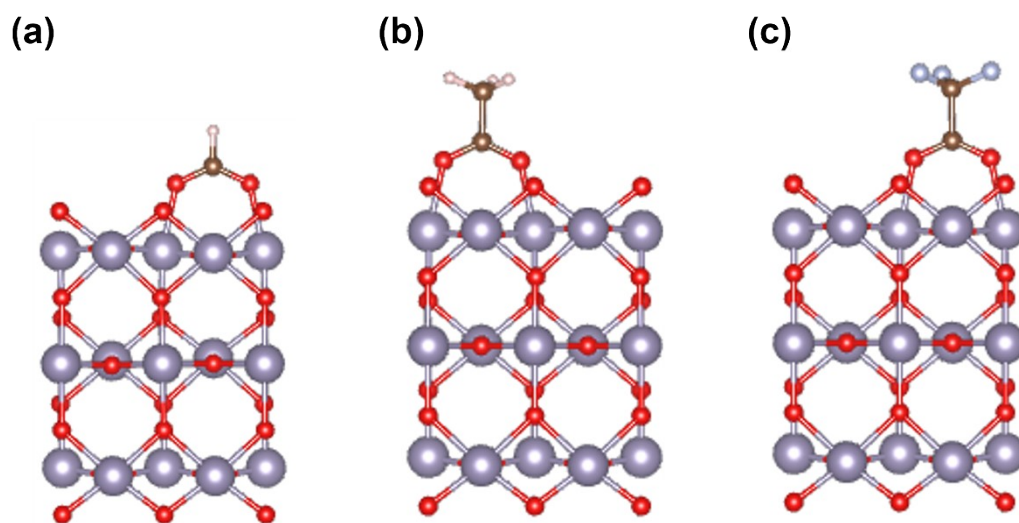
Fig. S11 Side view along [010] of (a) HCO_2, (b) CH_3CO_2, and (c) CF_3CO_2 molecules adsorbed on (111) SnO_2 slab. Atomic color scheme: Sn (gray), O (red), H (pink), C (brown), F (blue).
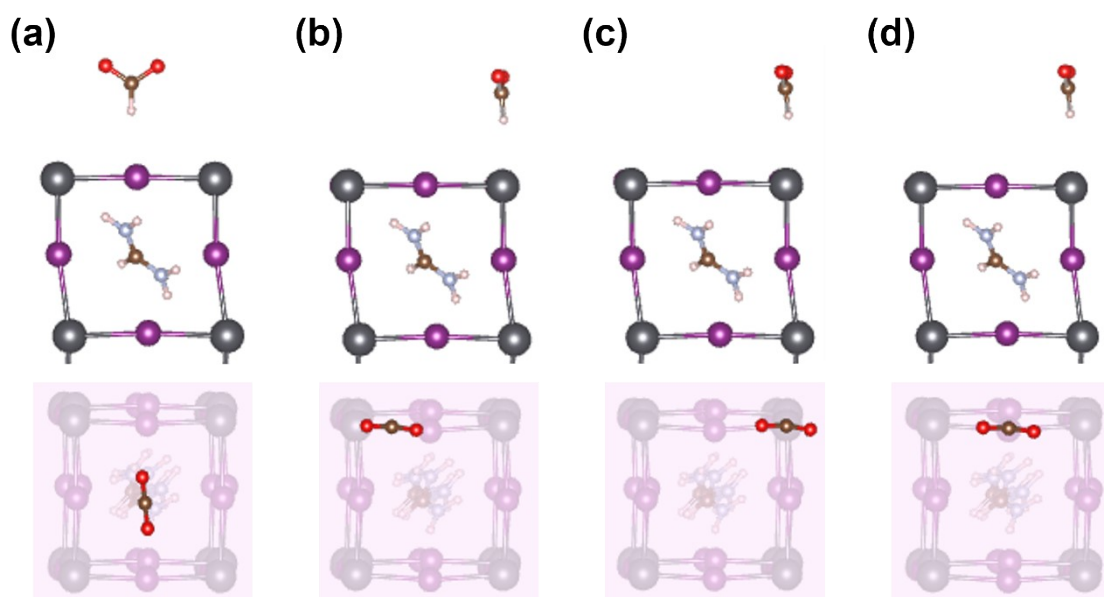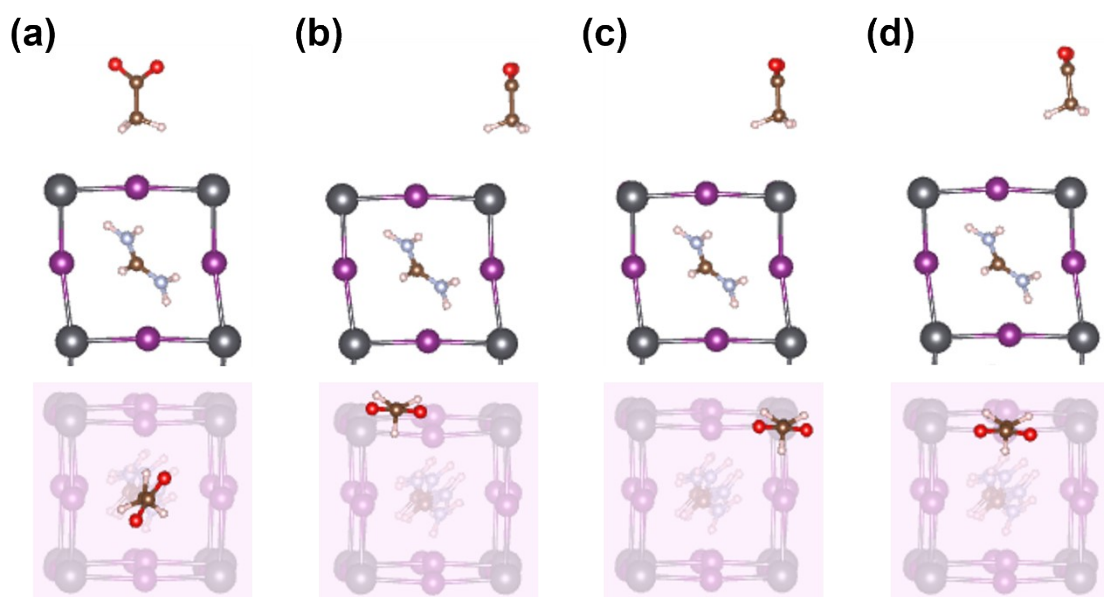
Fig. S12 Optimized structures of CO_2H molecules adsorbed on (a) I top, (b) Pb top, (c) hollow, and (d) Pb-I bridge sites of PbI_2-terminated $FAPbI_3$ perovskite.
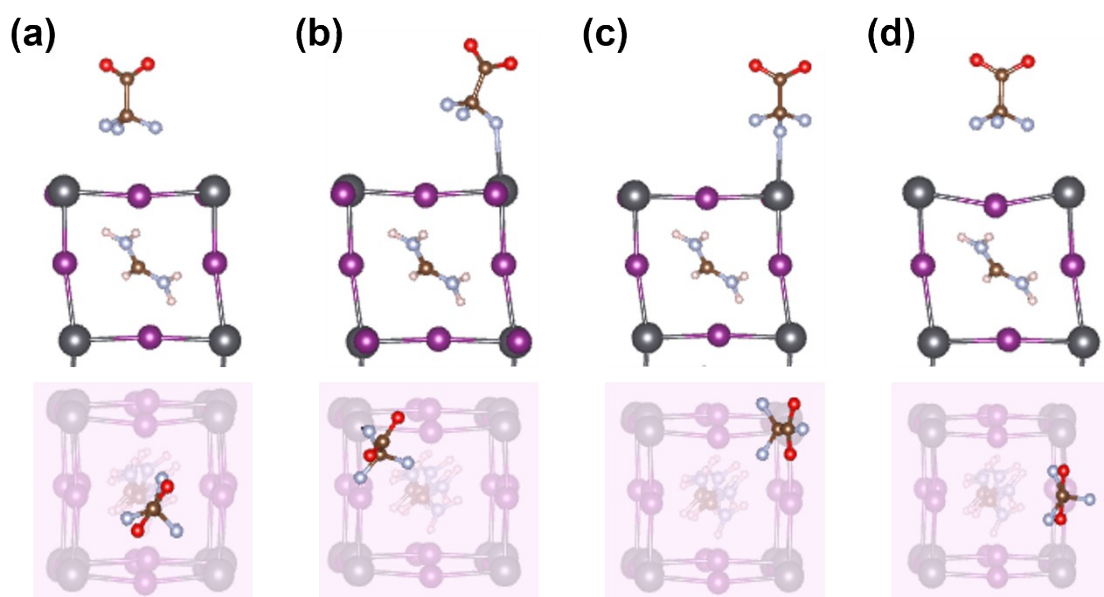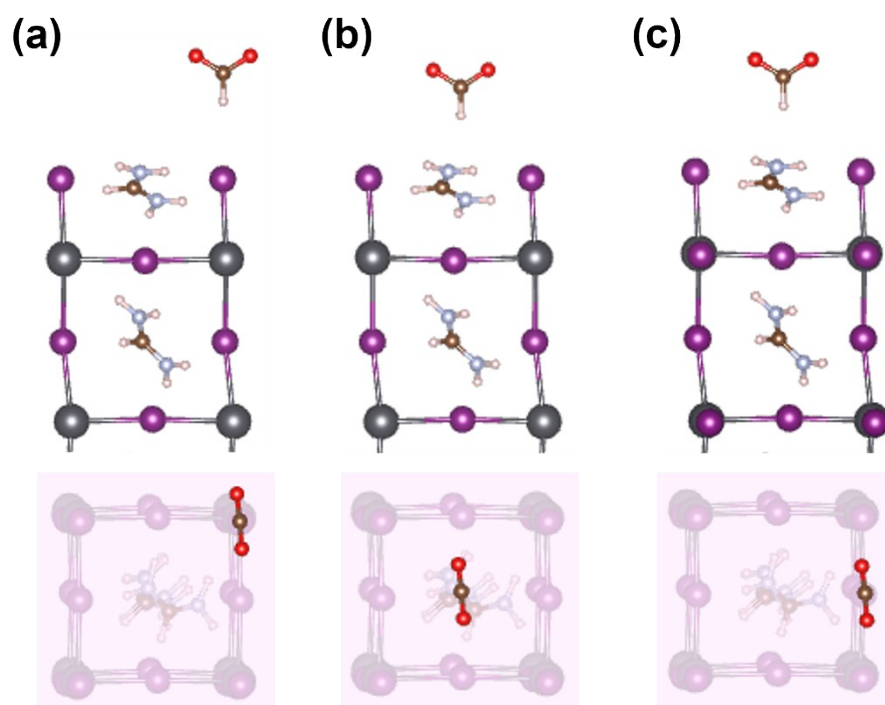
Fig. S13 Optimized structures of CO_2CH_3 molecules adsorbed on (a) I top, (b) Pb top, (c) hollow, and (d) Pb-I bridge sites of PbI_2-terminated $FAPbI_3$ perovskite.

Fig. S14 Optimized structures of CO_2CF_3 molecules adsorbed on (a) I top, (b) Pb top, (c) hollow, and (d) Pb-I bridge sites of PbI_2-terminated $FAPbI_3$ perovskite.

Fig. S15 Optimized structures of CO_2H molecules adsorbed on (a) I top, (b) hollow, and (c) I-I bridge sites of FAI-terminated $FAPbI_3$ perovskite.
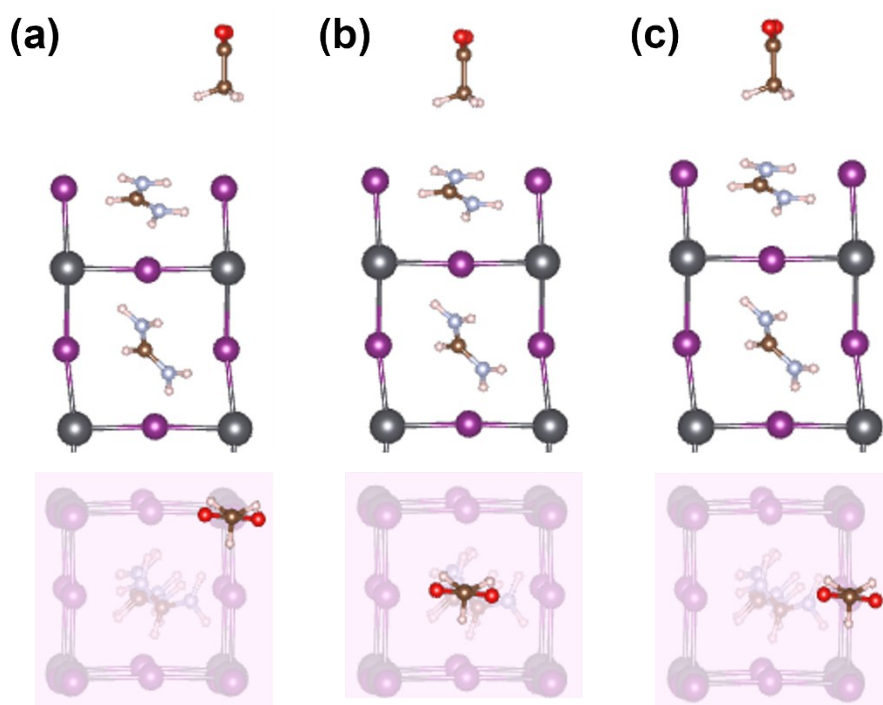
Fig. S16 Optimized structures of CO$_2$CH$_3$ molecules adsorbed on (a) I top, (b) hollow, and (c) I-I bridge sites of FAI-terminated FAPbI$_3$ perovskite.

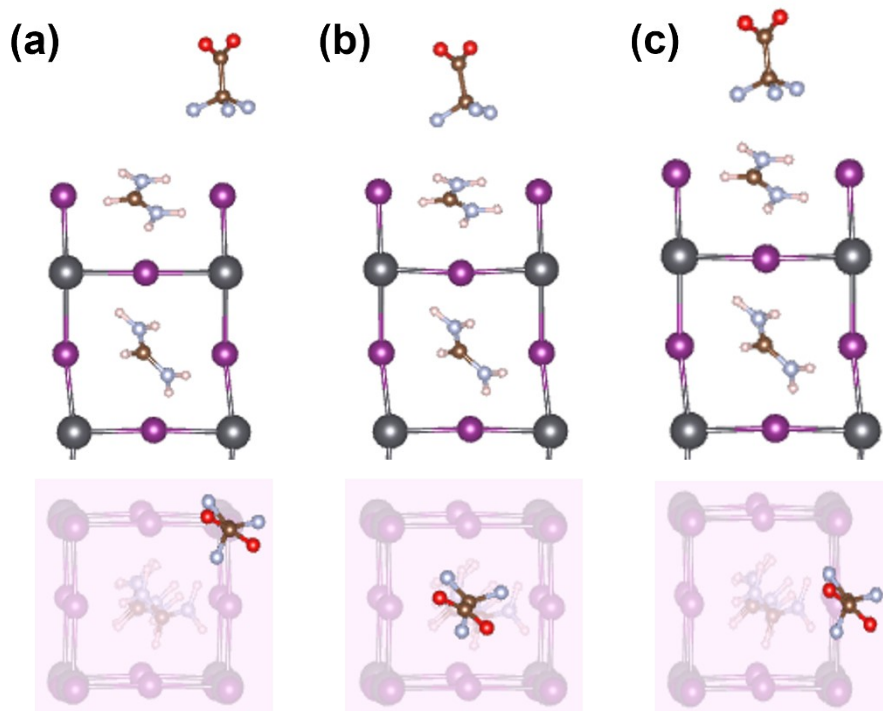**Fig. S17** Optimized structures of CO$_2$CF$_3$ molecules adsorbed on (a) I top, (b) hollow, and (c) I-I bridge sites of FAI-terminated FAPbI$_3$ perovskite.
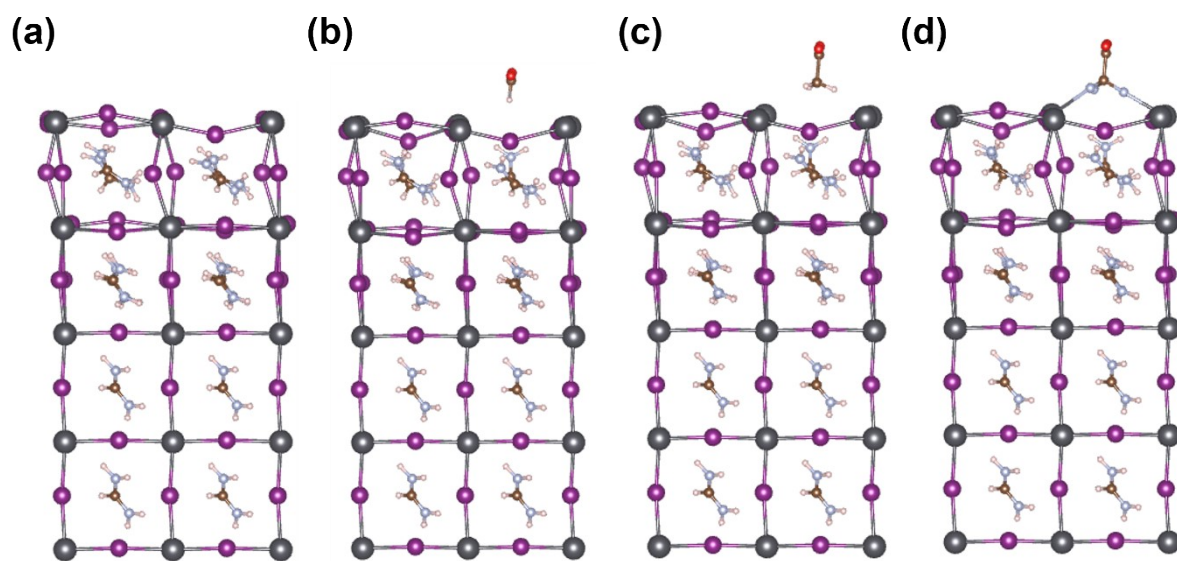
Fig. S18 Side views along [100] of (a) PbI_2-terminated (001) $FAPbI_3$ slab with iodine vacancy (V_i) surface defect and its interface with (b) HCO_2, (c) CH_3CO_2, and (d) CF_3CO_2 molecules. Atomic color scheme: Pb (gray), I (violet), N (blue), O (red), H (pink), C (brown), and F (blue).
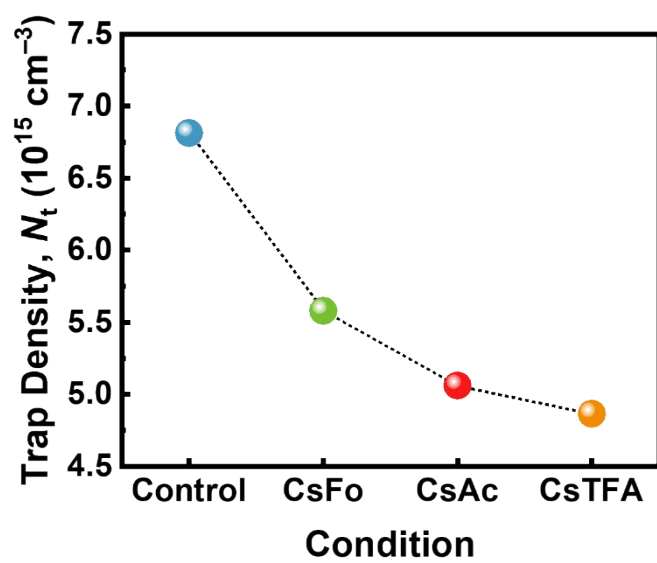
Fig. S19 Trap densities obtained from SCLC measurements of the perovskite films deposited on the control- and CsX-treated SnO_2.
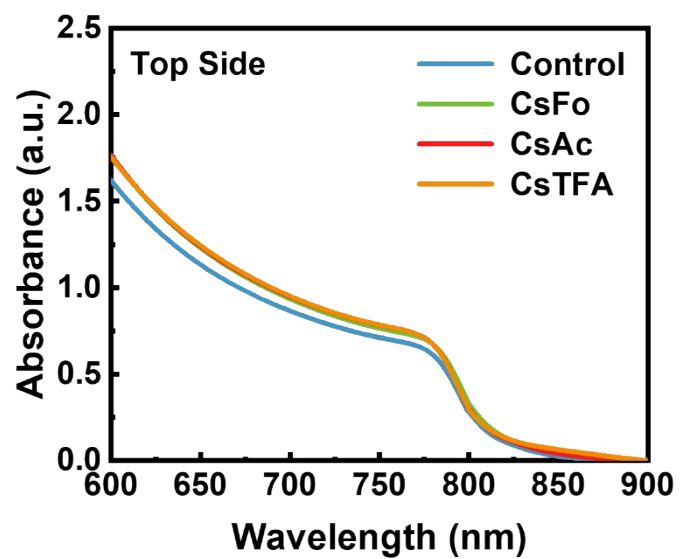
Fig. S20 Absorption spectra of the perovskite films deposited on the control- and CsX-treated SnO_2.
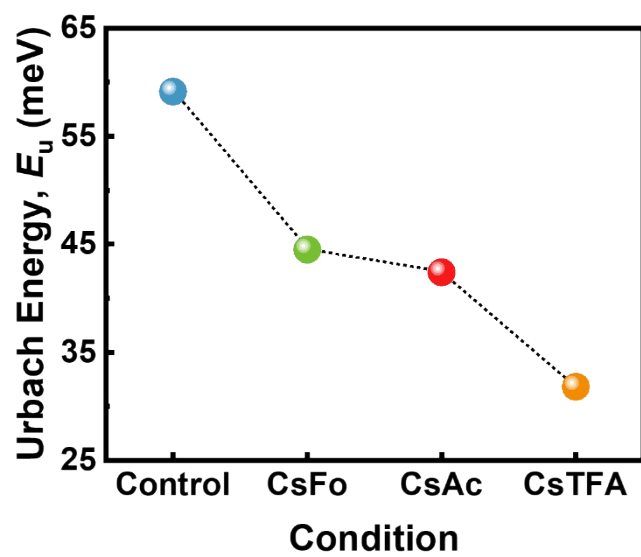
Fig. S21 Urbach energy (E_u) of the perovskite films deposited on the control- and CsX-treated SnO$_2$.
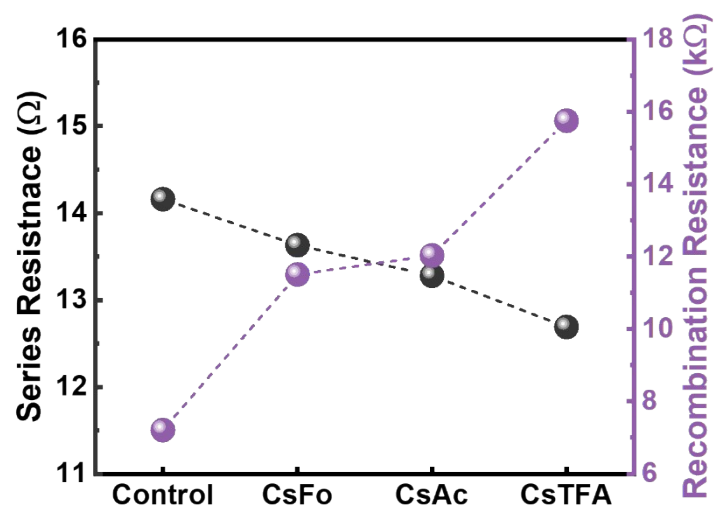
Fig. S22 Series resistance (R_s) and recombination resistance (R_{rec}) values obtained from EIS measurements of the devices using control- and CsX-treated SnO_2.
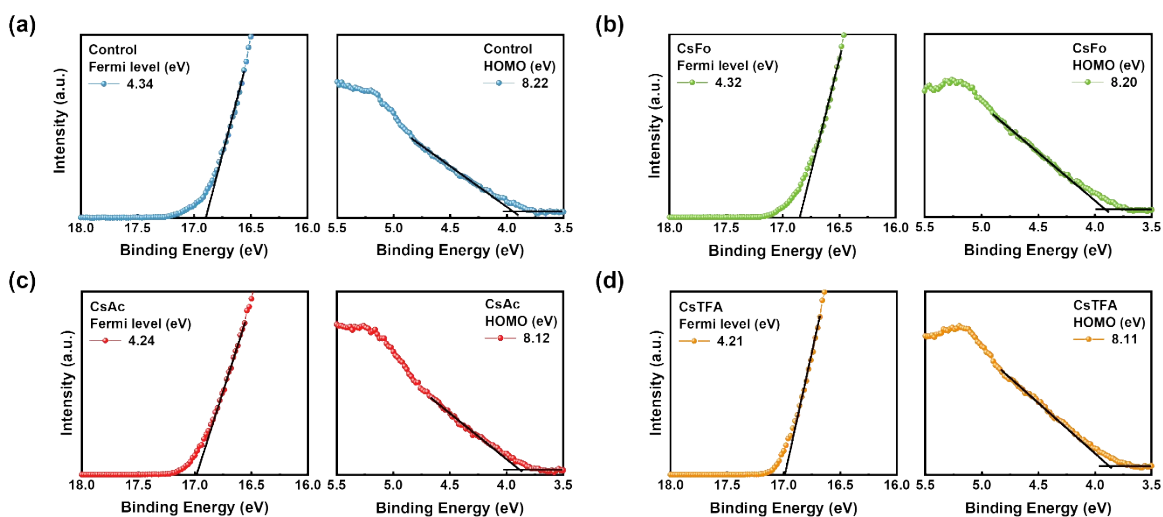
Fig. S23 UPS spectra of the (a) control-SnO_2, (b) CsFo-treated SnO_2, (c) CsAc-treated SnO_2, and (d) CsTFA-treated SnO_2; (left) secondary edge region and (right) valence band edge plotted relative to a gold reference.
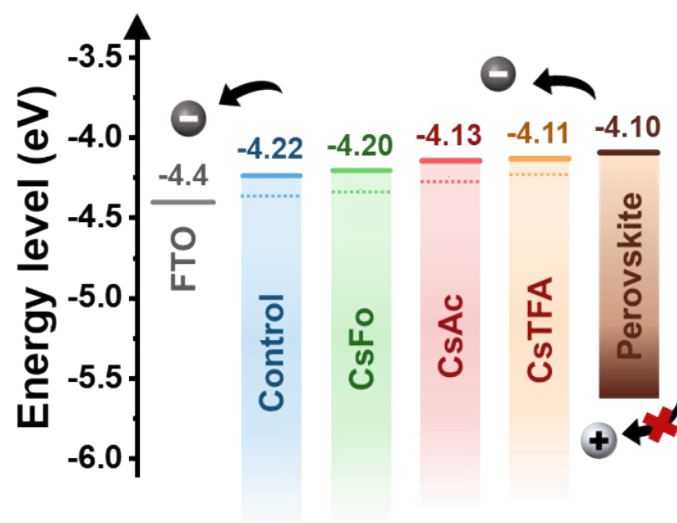
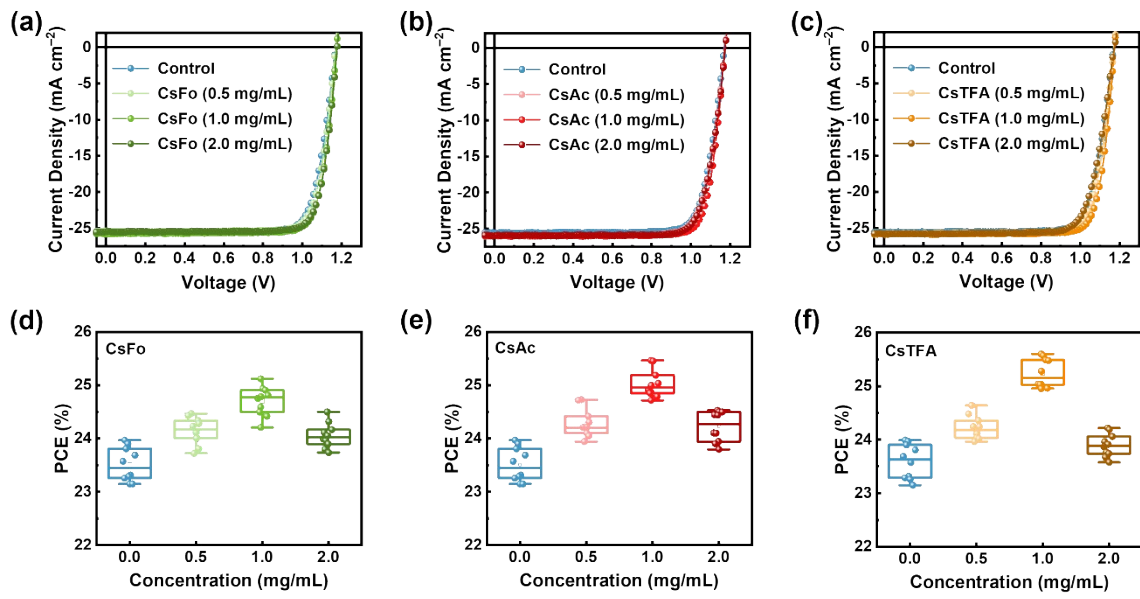**Fig. S24** Schematic diagram of the energy level alignment of the control- and CsX-treated SnO$_2$.

Fig. S25 *J-V* curves and statistic distribution of PCE of the PSCs with varying concentration of CsX, (a, d) CsFo, (b, e) CsAc, and (c, f) CsTFA.

DGTP 대구테크노파크 DAEGU TECHNOPARK **TEST REPORT** **DGTP**

46-17, Seongseo industrial Complex-ro,
Dalseo-gu, Daegu, Korea
(Tel: +82 53 602 1750 Fax: +82 53 602 1872)

Report No. : TP-NC-24S-0554
Page(2)/(2)Pages

· Test result
· 253904 : Area 0.0803 ㎠

	$V_{oc}(V)$	$I_{sc}(mA)$	$J_{sc}(mA/㎠)$	$F.F(\%)$	$I_{max}(mA)$	$V_{max}(V)$	$P_{max}(mW)$	Eff.(%)
Test result	1.1726	2.107	26.2398	82.52	2.0236	1.0076	2.0391	25.3904

IV Curve

Power

Check Certificate of Authenticity : +82 53 602 1750

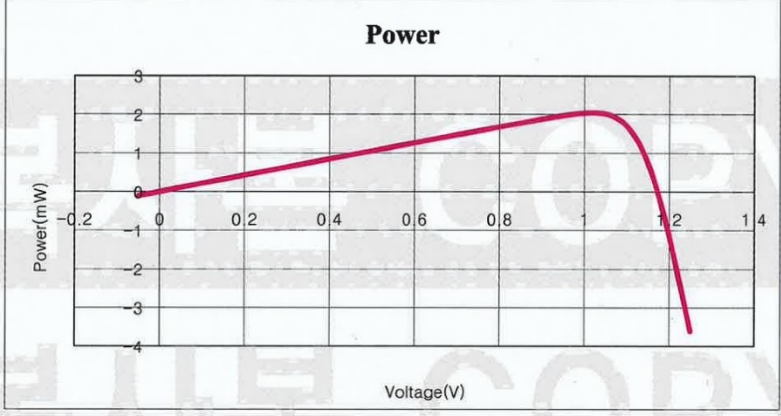NTPC-QP-15-T-06(01) Daegu Technopark Nanotechnology Processing Center A4(210 × 297)
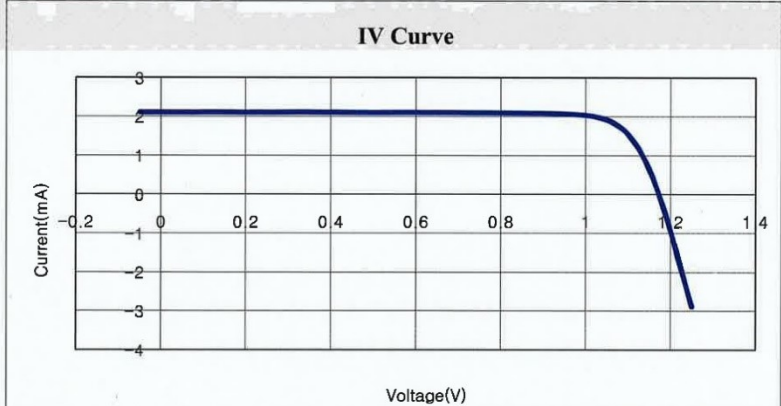
Fig. 26 Certificated PV performance for the photovoltaic with 0.0803 cm^2 active area from an accredited photovoltaic certification laboratory (Daegu Techpark, Republic of Korea). The certificated efficiency is 25.39%.
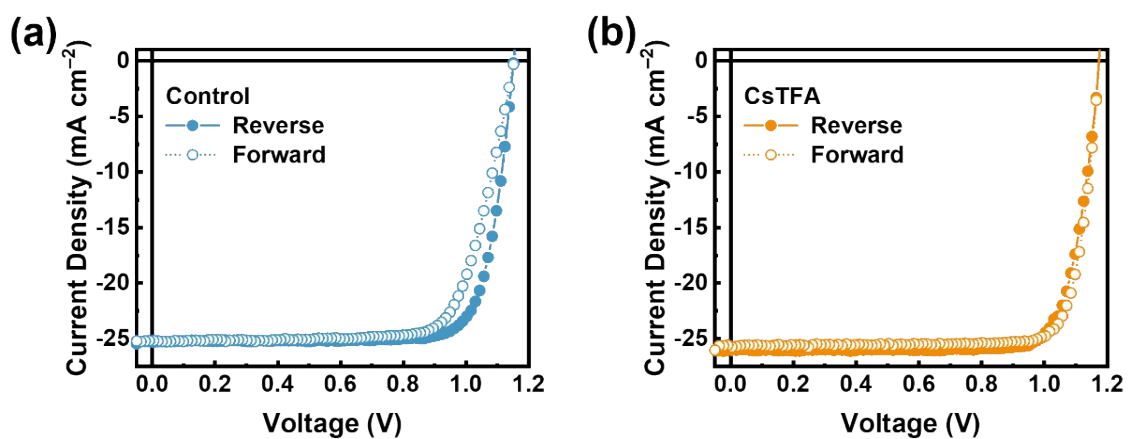
31

Fig. S27 *J-V* curves of the PSCs using the (a) control- and (b) CsTFA-treated SnO_2 under both reverse and forward scanning directions.
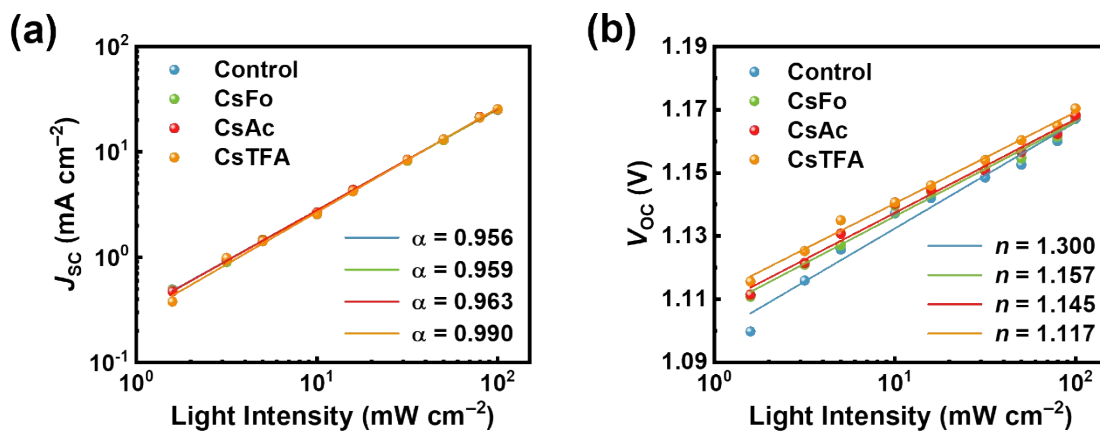
Fig. S28 The measured (a) J_{SC} and (b) V_{OC} with varying light intensity of the PSCs using the control- and CsX-treated SnO_2.
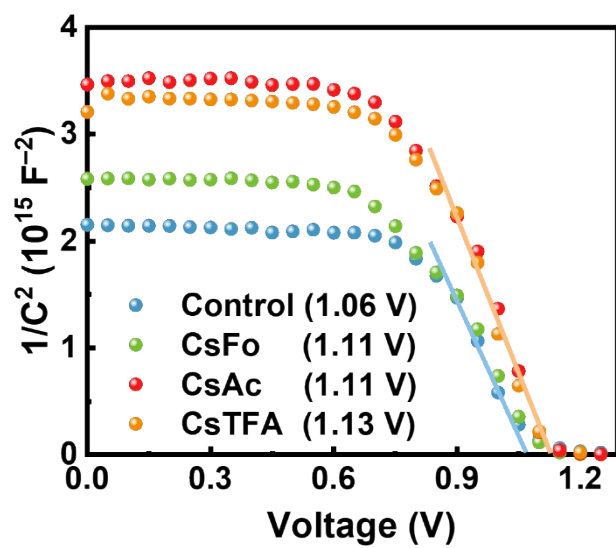
Figure S29 Mott-Schottky curves of the PSCs using the control- and CsX-treated SnO$_2$.
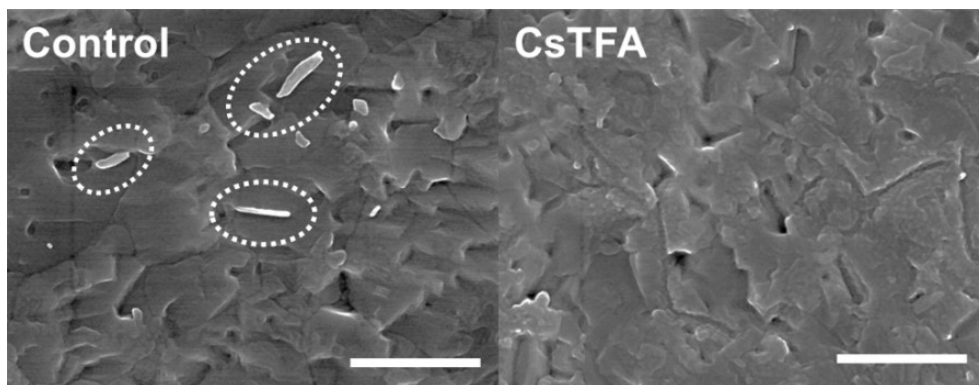
Fig. S30 SEM images of the perovskite films that were peeled off from the control- and CsTFA-treated SnO_2. (The scale bar is 1 μm).
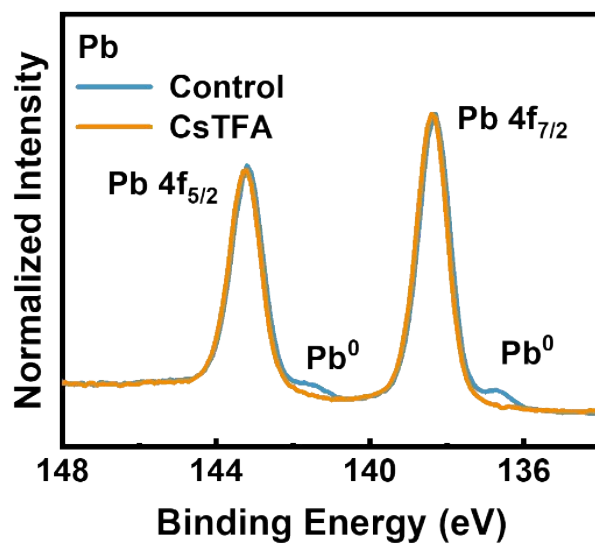
Fig. S31 XPS spectra corresponding to the Pb 4f peak of the perovskite films that were peeled off from the control- and CsTFA-treated SnO_2 after being subjected to 24 hours of light illumination.

Table S1. Summarized molecular adsorption energies of HCO_2, CH_3CO_2, and CF_3CO_2 molecules on I top, Pb top, hollow, Pb-I bridge sites of PbI_2-terminated $FAPbI_3$ perovskite.

Adsorption sites	Adsorption Energy (eV)			
	I_{top}	Pb_{top}	Hollow	Pb-I bridge
CsFo@FAPbI$_3$	-0.16	-0.14	-0.17	-0.20
CsAc@FAPbI$_3$	-0.16	-0.20	-0.19	-0.26
CsTFA@FAPbI$_3$	-0.42	-0.42	-0.47	-0.44

Table S2. Summarized molecular adsorption energies of HCO_2, CH_3CO_2, and CF_3CO_2 molecules on I top, hollow, I-I bridge sites of FAI-terminated $FAPbI_3$ perovskite.

Adsorption sites	Adsorption Energy (eV)		
	I_{top}	Hollow	I-I bridge
CsFo@FAPbI$_3$	-0.16	-0.17	-0.17
CsAc@FAPbI$_3$	-0.12	-0.14	-0.16
CsTFA@FAPbI$_3$	-0.42	-0.46	-0.49

Table S3. Summarized biexponential fitting parameters for time-resolved PL lifetimes of the perovskite films deposited on the control- and CsX-treated SnO_2.

ETL	τ_1 (ns)	f_1 (%)	τ_2 (ns)	f_2 (%)	τ_{avg} (ns)	χ^2
Control	435.34	40.11	121.61	59.89	247.45	1.07
CsFo	364.40	36.17	97.03	63.83	193.73	1.13
CsAc	329.63	27.62	85.89	72.38	153.21	1.00
CsTFA	251.85	24.50	67.27	75.50	108.71	0.98

Table S4. Detailed *J-V* parameters of the optimized PSCs using the control- and CsX-treated SnO$_2$ ETLs under reverse voltage scan.

Condition	V_{OC} (V)	J_{SC} (mA cm^{-2})	FF (%)	Integrated J_{SC} (mA cm^{-2})	PCE (%)
Control	1.171 (1.168±0.002)	25.78 (25.26±0.10)	78.71 (74.63 ±1.95)	25.30	23.77 (23.51±0.30)
CsFo	1.173 (1.171±0.002)	25.89 (25.31±0.05)	82.72 (80.99±0.55)	25.37	25.13 (24.70±0.26)
CsAc	1.174 (1.173±0.006)	25.98 (25.59±0.11)	83.48 (81.06±0.59)	25.78	25.46 (25.03±0.25)
CsTFA	1.175 (1.174±0.006)	26.00 (25.76±0.16)	83.81 (82.18±0.43)	25.98	25.60 (25.24±0.25)

Table S5. Detailed *J-V* parameters of the optimized PSCs using the control- and CsTFA-treated SnO$_2$ ETLs under both reverse and forward voltage scans.

Condition	Scan direction	V_{OC} (V)	J_{SC} (mA cm^{-2})	FF (%)	PCE (%)	HI
Control-SnO$_2$	Reverse	1.152	25.294	0.797	23.224	0.067
	Forward	1.153	25.186	0.746	21.663	
CsTFA-SnO$_2$	Reverse	1.173	26.003	0.832	25.377	0.015
	Forward	1.174	25.857	0.823	24.983	

Supplementary References

1. G. Kresse, J. Furthmüller. *Comput. Mater. Sci.*, 1996, **6**, 15–50.

2. J. P. Perdew, K. Burke, M. Ernzerhof. *Physical Review Letters*, 1996, **77**, 3865–3868.

3. S. Grimme, J. Antony, S. Ehrlich, H. Krieg. *The Journal of Chemical Physics*, 2010, **132**, 154104.

4. M. T. Weller, O. J. Weber, J. M. Frost, A. Walsh. *J. Phys. Chem. Lett.*, 2015, **6**, 3209–3212.

5. C. Zhu, X. Niu, Y. Fu, N. Li, C. Hu, Y. Chen, X. He, G. Na, P. Liu, H. Zai, Y. Ge, Y. Lu, X. Ke, Y. Bai, S. Yang, P. Chen, Y. Li, M. Sui, L. Zhang, H. Zhou, Q. Chen, *Nat. Commun.* 2019, **10**, 815.

6. L. Guo, G. Tang, J. Hong, *Chinese Phys. Lett.* 2019, **36**, 056201.